

Electrochemical Corrosion Behavior of 2205 Duplex Stainless Steel Welds in Chloride Solutions

HaiTao Yan^{1,2}, SenSen Xin², Yong Yang¹, Sai Yang², MouCheng Li^{1,*}

¹ Institute of Materials, School of Materials Science and Engineering, Shanghai University, 149 Yanchang Road, Shanghai 200072, China

² Zhenshi Group Eastern Special Steel CO., LTD., Jiaxing 314005, Zhejiang Province, China

*E-mail: mouchengli@shu.edu.cn

Received: 2 October 2018 / Accepted: 19 November 2018 / Published: 5 January 2019

The microstructure and corrosion behavior of 2205 duplex stainless steel (DSS) welds were investigated by optical microscopy (OM), scanning electronic microscopy (SEM) and electrochemical measurements. The ferrite (δ) phase content increases slightly from the base metal (BM) zone, to the heat affected zone (HAZ) to the weld metal (WM) of the welded joint. HAZ shows a very weak sensitization that was effectively detected by the double-loop electrochemical potentiokinetic reactivation (DL-EPR) test with an $\text{H}_2\text{SO}_4 + \text{HCl}$ mixed solution. In hot artificial seawater, the pitting corrosion resistance, passivation and repassivation abilities decrease gradually from BM, to WM to HAZ. Weak sensitization plays a dominant role in the pitting corrosion of HAZ even though the degree of sensitization (DOS) is very low. BM and WM do not show intergranular corrosion (IGC) susceptibility and the difference in the pitting resistance between these two zones is small. The pitting corrosion resistance of the three weld zones was discussed in detail.

Keywords: Duplex stainless steel, welding, pitting corrosion, intergranular corrosion, seawater

1. INTRODUCTION

Duplex stainless steels (DSSs) have been widely used in many aggressive environments due to their excellent combination of mechanical properties and corrosion resistance [1-3]. Generally, such good properties depend strongly on obtaining the microstructures with approximately equal amounts of austenite (γ) and ferrite (δ) phases, and absence of secondary phases such as sigma and Cr_2N [4-7].

In the industrial applications of DSSs, welding is commonly adopted in their fabrication processes. It is known that the welding fabrication must exert cyclic heating and cooling effects on the DSS microstructures. For example, the grain coarsening and the formation of undesired precipitates such

as Cr_2N , M_{23}C_6 , secondary austenite (γ_2) and sigma phase often occur in the heat-affected zone (HAZ) [8-10]. These effects may dramatically deteriorate the mechanical properties and localized corrosion resistance of DSSs [11-14]. Pitting corrosion occurs preferentially at the Cr-depleted regions adjacent to the Cr_2N precipitates or at the γ_2 regions with low Cr and Mo contents in the HAZ [8,15,16]. Typically, welding parameters such as heat input, interpass temperature and postweld heat treatment (PWHT) play important roles in the mechanical and corrosion properties of welded joints [17-20]. The secondary phase precipitation can be dissolved by PWHT to improve the pitting corrosion resistance [13,14]. Therefore, it is necessary to evaluate the corrosion resistance of the welded joints in order to determine the optimal welding procedure prior to the practical applications of DSSs.

Double loop electrochemical potentiokinetic reactivation (DL-EPR) tests provide a quantitative method for detecting intergranular corrosion (IGC) susceptibility in welded components. Mixed solutions of H_2SO_4 and HCl have been used effectively in DL-EPR tests for rapid and reliable measurements of the degree of sensitization (DOS) of DSSs [1]. With the increasing application of DSSs in aqueous chloride environments such as in desalination plants [21,22], the effect of sensitization on their pitting corrosion tendency has attracted intense attention. In this work, the electrochemical behavior of the different zones of 2205 DSS weld was investigated using the DL-EPR and cyclic anodic polarization tests to examine IGC and pitting corrosion, respectively. The main goal of this work is to characterize the weak sensitization as well as its influence on the pitting resistance of the 2205 DSS welds in seawater.

2. EXPERIMENTAL

2.1 Materials and welding parameters

The base metal was a 2205 DSS sheet with a thickness of 8.0 mm and the filler wire was ER2209 with a diameter of 1.2 mm. Their chemical compositions are given in Table 1. Prior to welding, the V-shape groove was machined using a milling machine, as shown in Fig. 1a. The plates were welded using gas tungsten arc welding (GTAW) in the 98% Ar + 2% N_2 shielding gas, with a schematic diagram of the two-pass welding process shown in Fig. 1b. The welding heat input (Q) was approximately 0.72 kJ mm^{-1} , as obtained according to $Q = \eta UI/S$ [8] with the current $I = 290 \text{ A}$, voltage $U = 18 \text{ V}$, speed $S = 4.7 \text{ mm min}^{-1}$, and thermal efficiency $\eta = 0.65\%$. The interpass temperature was controlled at $<150 \text{ }^\circ\text{C}$.

Table 1. Chemical compositions of the 2205 DSS and filler wire (wt.%)

Material	C	Si	Mn	P	S	Cr	Ni	Mo	N	Fe
2205	0.028	0.51	1.44	0.021	0.0015	22.05	5.45	3.2	0.16	Bal.
ER2209	0.020	0.49	1.40	0.020	0.0050	22.90	8.50	3.1	0.16	Bal.

The specimens with the dimensions of $10 \text{ mm} \times 5 \text{ mm} \times 8 \text{ mm}$ were cut from the three zones of welded joints, i.e., base metal (BM), weld metal (WM) and heat affected zone (HAZ). The HAZ

specimens inevitably contain small regions of BM and WM. All of the specimens were embedded in an epoxy resin. Prior to each measurement, the working surface on the weld cap side was ground with successive grade silicon carbide sandpaper up to 1000 grit, degreased with ethanol, rinsed with distiller water and dried in air.

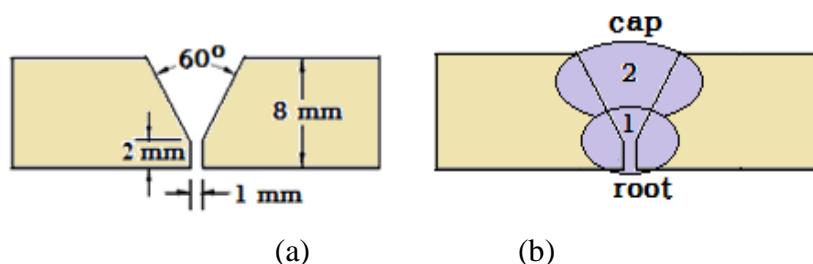


Figure 1. Schematic diagrams of (a) the V-shape groove and (b) two passes for welding process

2.2 Microstructure characterization

To optically observe the microstructure of the welded joints from the cap side, the samples were ground with successive grade abrasive papers up to 1200 grit, and polished by 1.5 μm diamond paste. Then the samples were electrochemically etched in a 30 wt.% KOH solution with an etching potential of 2 V for 15 s. The volume fraction of the δ phase was evaluated using ferrite indicator (Fischer MP30), and the microstructure was characterized by optical microscopy (OM, Axio Imager A2m).

2.3 Electrochemical measurements

A classical three-electrode cell was used for electrochemical measurements. The specimen was used as the working electrode, a platinum plate with an area of 2 cm^2 as the counter electrode and a saturated calomel electrode (SCE) with a long Luggin capillary as the reference electrode. All of the potential values here were relative to SCE. The measurements were performed using a PAR system (Princeton Application Research) consisting of a potentiostat/galvanostat (M273A) and the Powersuite software.

DL-EPR tests were conducted in a mixed solution of 1 $\text{mol}\cdot\text{L}^{-1}$ H_2SO_4 + 1.5 $\text{mol}\cdot\text{L}^{-1}$ HCl at 30 $^\circ\text{C}$ with a scan rate of 1.66 $\text{mV}\cdot\text{s}^{-1}$. The test was started by a potential sweep in the anodic direction from the corrosion potential (E_{corr}) until the potential reached +0.3 V_{SCE} . Then the scan was reversed in the cathodic direction until the potential reached E_{corr} . During the forward and reverse scans, the activation current density (I_a) and reactivation current density (I_r) were measured. DOS was calculated as $(I_r/I_a) \times 100\%$ [1].

Cyclic polarization tests were performed in artificial seawater (i.e., 3.5% NaCl) at 70 $^\circ\text{C}$ to simulate the conditions of thermal desalination processes [23]. The specimen was immersed in artificial seawater for 1 h to attain a steady corrosion state. The polarization curve was then measured from E_{corr} in the anodic direction with a scan rate of 20 $\text{mV}\cdot\text{min}^{-1}$. The scanning direction was reversed when the

current density reached $1 \text{ mA}\cdot\text{cm}^{-2}$. In the cyclic polarization curve, the pitting potential (E_{pit}) is defined as the potential at which the passive film is destroyed and intense localized attack takes place, and the protection potential (E_{pro}) is defined as the potential at which the current density in the forward scan is equal to that in the reverse scan. The passive current density (i_p) is obtained at $0.1 \text{ V}_{\text{SCE}}$ between E_{corr} and E_{pit} .

To ensure reproducibility, each electrochemical experiment was performed in triplicate. After the above-described tests, the surface morphology of the specimens was examined by scanning electronic microscopy (SEM, Hitachi S3400N).

3. RESULTS AND DISCUSSION

3.1 Microstructure characteristics of the welded joint

Fig. 2 shows an optical micrograph of the welded joint that can be divided into three zones, i.e., BM, HAZ and WM. In the BM zone, the white area is the γ phase, and the gray area is the δ phase. The volume fractions of the δ and γ phases are approximately 51.9% and 48.1%, respectively, indicating a good δ/γ phase balance. HAZ has almost the same micrograph as the BM zone, but with a higher volume fraction of the δ phase (approximately 53.2%).

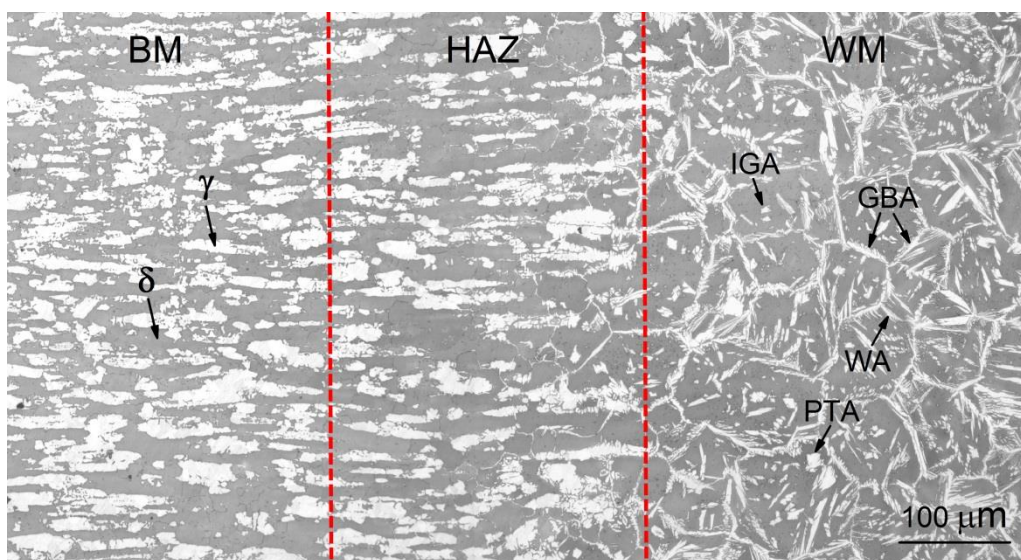


Figure 2. Optical microstructure of the three zones for the welded joint: base metal (BM), heat affected zone (HAZ) and weld metal (WM).

This can be attributed to the difference between the effective quench temperatures [24]. It is clear that during welding, the area in the vicinity of the fusion line has a higher effective quench temperature than the area far from the fusion line, leading to the high δ content. According to the literature [25,26], small amounts of γ_2 and Cr_2N must precipitate in HAZ as it is reheated during the welding thermal cycle; however, these phases cannot be identified in Fig. 2. In the WM zone, the microstructures consist of four

kinds of austenite phases, i.e., grain boundary austenite (GBA), Widmännstten-type austenite (WA), intragranular austenite (IGA) and partially transformed austenite (PTA) [8,27]. The volume fractions of the δ and γ phases in this zone are approximately 58.5% and 41.5%, respectively. Clearly, the volume fraction of the δ phase increases slightly from the BM, to HAZ and then to WM, with the volume fraction difference of less than 6.6% only.

3.2 Susceptibility to IGC

To evaluate the IGC susceptibility of the welded joint, the DL-EPR curves for the three zones in $1 \text{ mol}\cdot\text{L}^{-1} \text{H}_2\text{SO}_4 + 1.5 \text{ mol}\cdot\text{L}^{-1} \text{HCl}$ solution at 30°C were obtained and are shown in Fig. 3. Both BM and WM show no reactivation peak in the reverse scans, indicating no IGC susceptibility. HAZ has a small reactivation peak with a current density of approximately $2.2 \mu\text{A}\cdot\text{cm}^{-2}$. It is calculated that the DOS value is approximately 0.026%. This implies the occurrence of very weak sensitization in HAZ during the welding. Fig. 4 shows the SEM morphologies of the specimen surfaces after the DL-EPR tests. It is observed that the slight IGC occurred along the grain boundaries on the HAZ surface, but no IGC was found on both the BM and WM surfaces.

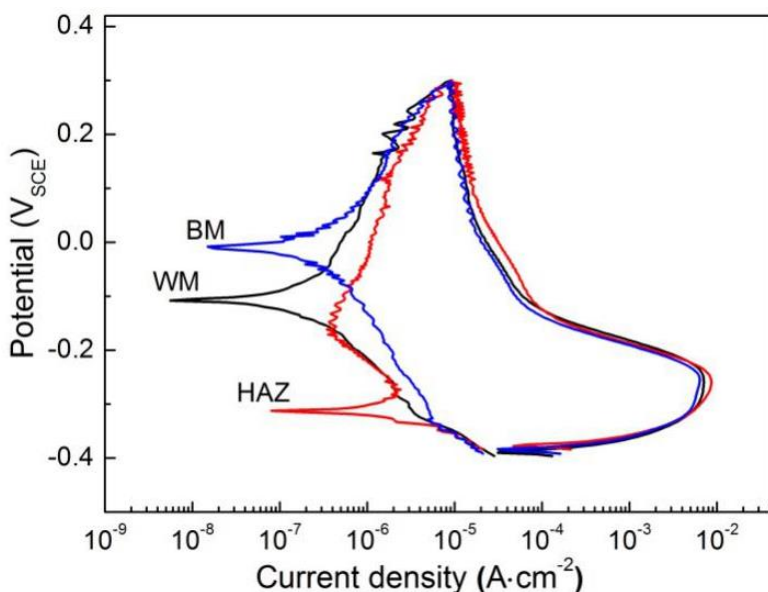


Figure 3. DL-EPR curves for the three zones of the welded joint in the solution $1 \text{ mol}\cdot\text{L}^{-1} \text{H}_2\text{SO}_4 + 1.5 \text{ mol}\cdot\text{L}^{-1} \text{HCl}$ at 30°C

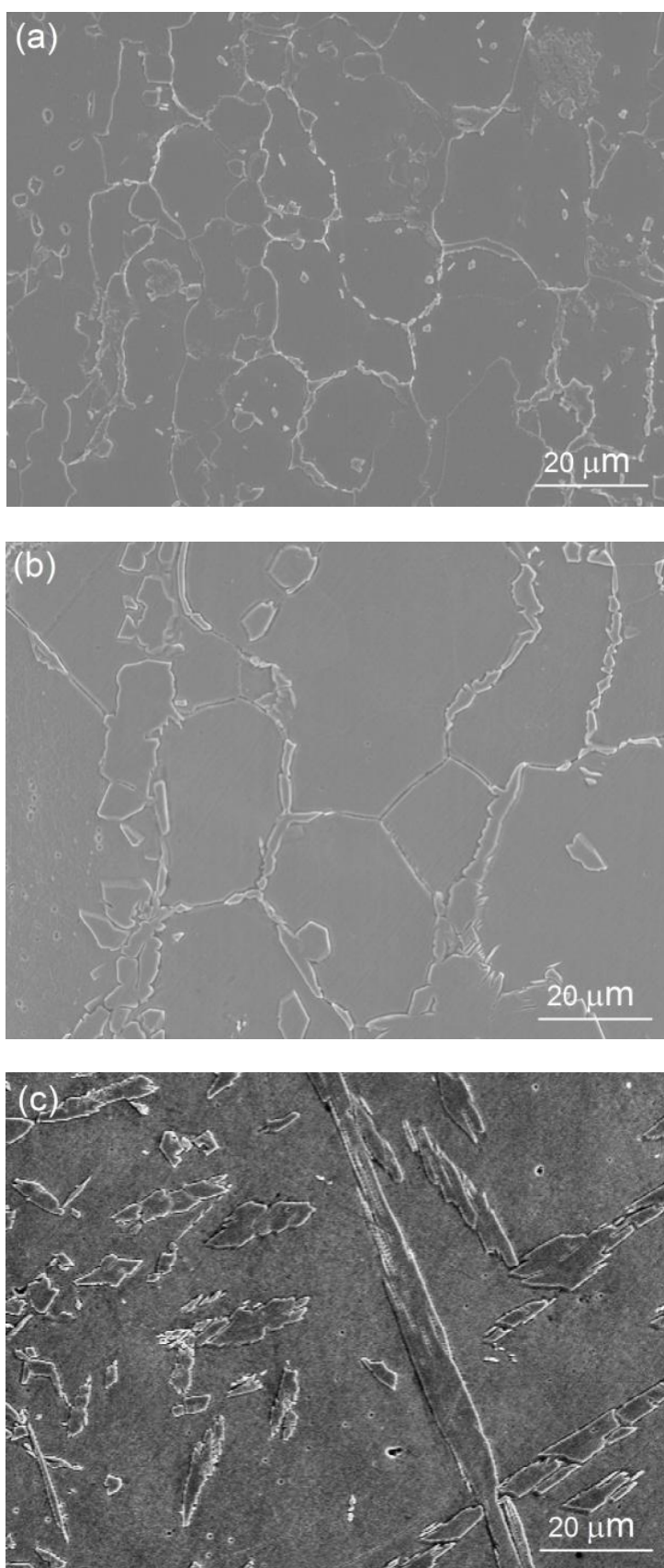


Figure 4. SEM morphologies of the specimens after the DL-EPR tests: (a) BM, (b) HAZ and (c) WM

According to the literature [8,15], the peak temperature for HAZ could reach above 1000 °C. Due to the rapid cooling after the welding, the ferrite became supersaturated in nitrogen and the Cr₂N precipitated either along the grain boundaries or at the ferrite regions. The intergranular Cr₂N is likely to be mainly responsible for the Cr-depletion and the ensuing weak sensitization in HAZ observed here [15]. It will likely be difficult to prevent such weak sensitization by optimizing the welding parameters in practical use.

During the DL-EPR test, the specimen was first polarized from the corrosion potential to an anodic potential of 0.3 V_{SCE} in the passive region, leading to the formation of a passive film on the entire surface. Then, the electrode potential was decreased from 0.3 V_{SCE} to the corrosion potential, resulting in the breakdown of the passive film on the Cr-depleted regions of HAZ [28]. In addition, HCl acted as a depassivator in the mixed solutions and promoted the dissolution of the passive film on the Cr-depleted region. In this case, the HCl concentration is suitable for detecting the very weak sensitization in HAZ without producing strong uniform corrosion on the entire specimen surface and reactivation in the BM zone. Furthermore, the Cr-depletion occurred only in the vicinity of the small amount of Cr₂N precipitates in HAZ. These are mainly responsible for the very low DOS value of approximately 0.026%.

3.3 Resistance to pitting corrosion

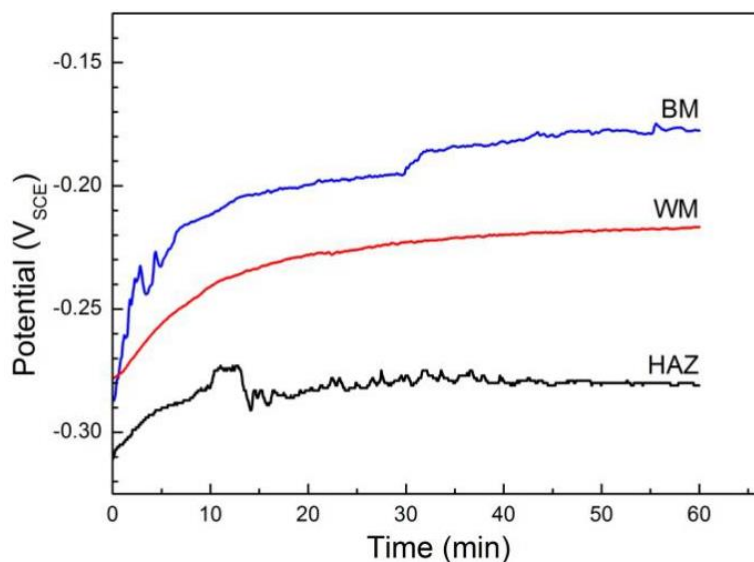


Figure 5. Variation of the corrosion potential with time for the specimens in the solution 3.5% NaCl at 70 °C

The electrochemical corrosion behavior was investigated in a 3.5% NaCl solution for the three zones in order to evaluate the pitting resistance of the welded joint. Fig. 5 shows the variation of E_{corr} with time during immersion for 1 h. E_{corr} for each specimen increases with time, indicating the gradual formation of a passive film on the surface. After 1 h of immersion, the corrosion attains a steady state with stable E_{corr} values of -0.178 , -0.216 and -0.280 V_{SCE} for the BM, WM and HAZ, respectively. It is clear that E_{corr} changes to the cathodic direction from the BM to HAZ, with a reduction of approximately 102 mV. This can be mainly attributed to the different passive films forming on the three

zones. HAZ formed a less protective passive film on the surface than the BM and WM, as confirmed by the i_p values in Table 2.

Fig. 6 shows the cyclic polarization curves for the three weld zones. The anodic curves have the loop characteristic of pitting corrosion. This indicates that the pits induced on the three zones can repassivate as the electrode potential decreases to E_{pro} .

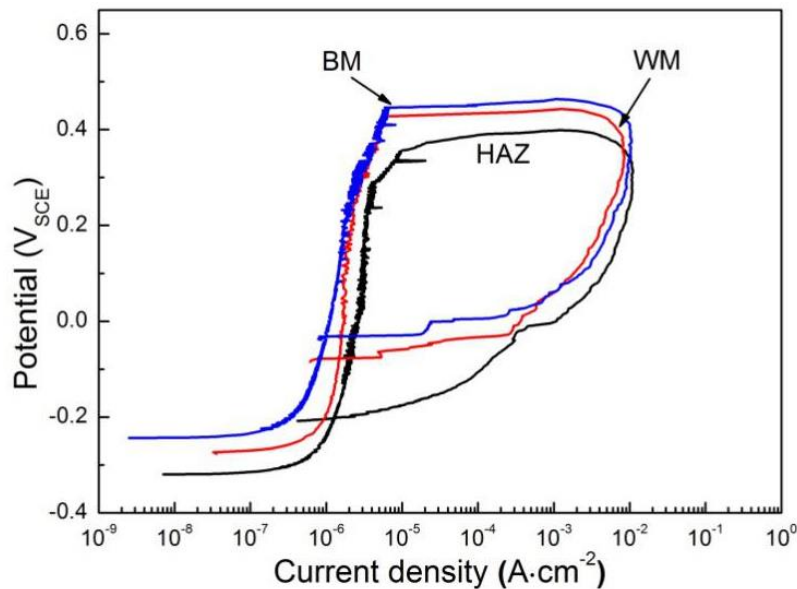


Figure 6. Cyclic polarization curves for the specimens in the solution 3.5% NaCl at 70 °C

Table 2 lists the values for the electrochemical parameters obtained from the cyclic polarization curves. It is observed that the average E_{pit} values are approximately 0.445, 0.427 and 0.355 V_{SCE} for BM, WM and HAZ, respectively. Both BM and WM exhibit higher E_{pit} than HAZ, indicating that HAZ is the weak zone resistant to pitting corrosion. HAZ has an average i_p value of approximately 3.11 $\mu\text{A}\cdot\text{cm}^{-2}$, which is much higher than those of the other weld zones. Therefore, HAZ shows the most unstable passive state among the three zones. This is largely responsible for the lower resistance of HAZ to pitting corrosion compared to WM and BM.

Table 2. Electrochemical parameters in hot artificial seawater

Specimen	i_p ($\mu\text{A}\cdot\text{cm}^{-2}$)	E_{pit} (V _{SCE})	E_{pro} (V _{SCE})	$E_{pit}-E_{pro}$ (V)
BM	1.43 ± 0.037	0.445 ± 0.007	-0.032 ± 0.007	0.477 ± 0.001
WM	1.74 ± 0.049	0.427 ± 0.006	-0.076 ± 0.006	0.503 ± 0.001
HAZ	3.11 ± 0.054	0.355 ± 0.009	-0.203 ± 0.011	0.558 ± 0.003

The average E_{pro} values are approximately -0.032 , -0.076 and -0.203 V_{SCE} for BM, WM and HAZ, respectively. HAZ exhibits the lowest repassivation ability among the three weld zones. The potential difference between E_{pit} and E_{pro} ($\Delta E = E_{pit} - E_{pro}$) is often used to estimate the susceptibility of metallic materials to pitting corrosion. It was concluded that HAZ is more susceptible to pitting corrosion

because of its higher ΔE value compared with the other zones. This is confirmed by SEM images for three zones after cyclic polarization measurements presented in Fig. 7. Compared with the BM and WM, HAZ has more and larger corrosion pits on the surface.

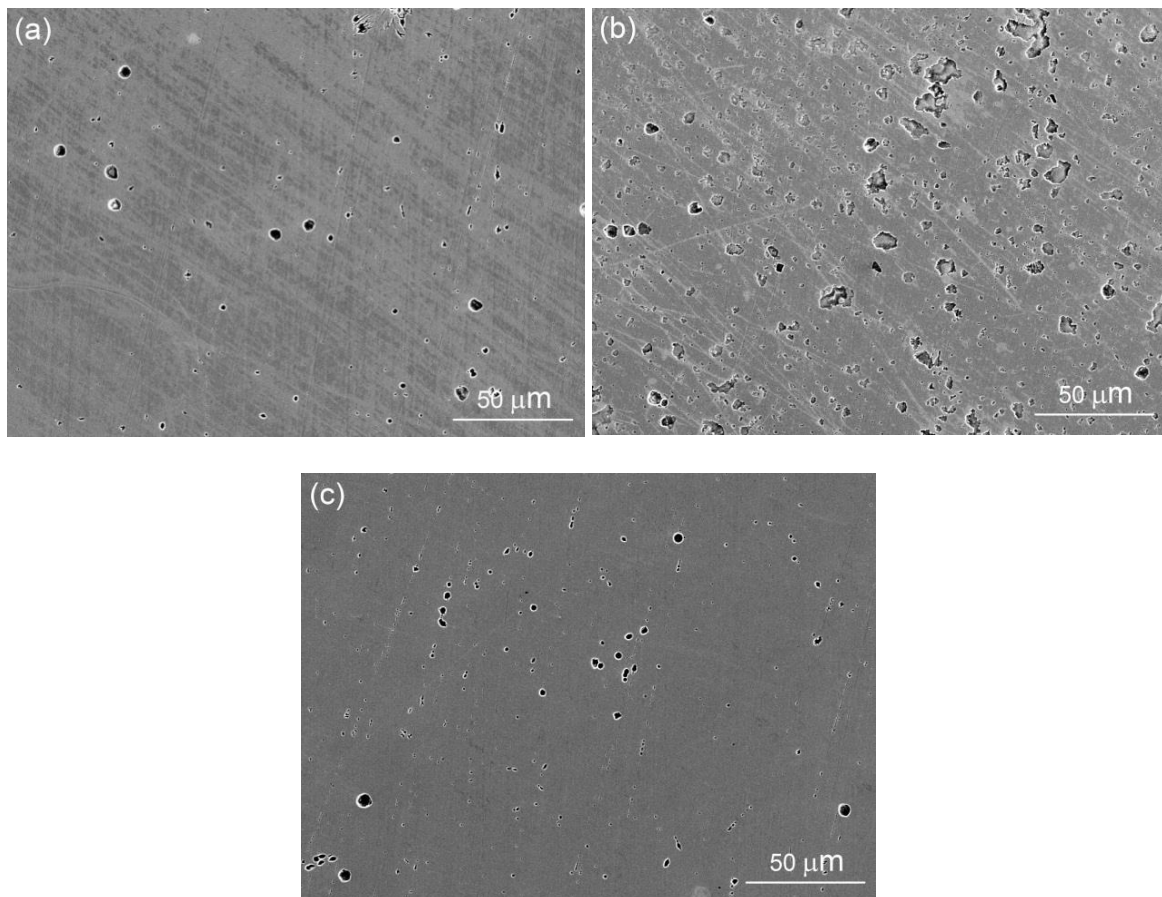


Figure 7. SEM surface images of the different weld zones after cyclic polarization measurements: (a) BM, (b) HAZ, (c) WM

It is observed from above results that the E_{corr} , E_{pit} and E_{pro} values decrease in the order of BM, WM and HAZ, while the i_p value increases in the same order. These results indicate that the pitting corrosion resistance, passivation and repassivation properties worsen in the order of BM, WM and HAZ. That is, HAZ has the worst pitting corrosion resistance among the three zones. This may be related to the following adverse features. First, weak Cr-depletion occurs together with Cr_2N precipitation in HAZ during the welding process, resulting in the DOS value of approximately 0.026%. The i_p values in Table 2 indicate that the weak passive films must form on the Cr-depleted regions and then provide the precursor sites for pitting corrosion. This is similar to the observations reported in the literature [8,15,29]. Second, a small amount of the γ_2 phase will precipitate together with the Cr_2N . The corrosion pits initiate preferentially at the γ_2 phase due to its lower Cr and Mo contents [30,31], but the nitrogen from the shielding gas greatly improves the pitting resistance equivalent number (PREN) of the γ_2 phase [8]. Third, the balance of γ - and δ -phases is altered slightly for the welded zones. WM has a higher δ phase content (approximately 5.3%) than HAZ, which may lead to lower pitting corrosion resistance [8]. In contrast, it is evident from the data in Table 2 that WM shows better pitting corrosion resistance than

HAZ. Clearly, despite the very small DOS value, the weak Cr-depletion, rather than the undesired γ_2 precipitates and imbalance in the microstructure, must play a dominant role in the pitting corrosion of HAZ.

The PREN values for WM and BM are approximately 34.3 and 33.7, respectively, as obtained using $\text{PREN} = \%Cr + 3.3\%Mo + 16\%N - Mn\%$. This suggests that WM has a slightly higher resistance to pitting corrosion than BM. However, as shown in Table 2, the opposite electrochemical results were obtained. WM shows lower E_{pit} and E_{pro} values than BM, corresponding to a slightly more poor pitting resistance. This can be ascribed mainly to its higher δ phase content (approximately 6.6%). Fortunately, the difference in the pitting resistance between the two zones is small as shown by the PREN values and electrochemical parameters.

4. CONCLUSIONS

It was found that the dual-phase balances in the HAZ and WM of 2205 DSS weld joint are degraded to some extent after welding in the 98% Ar + 2% N₂ shielding gas. The volume fraction of the δ phase increases slightly from BM, to HAZ to WM, but the volume fraction difference is less than 6.6%. HAZ shows a very weak sensitization that can be attributed mainly to a small amount of intergranular Cr₂N precipitated during the welding process. The small DOS can be detected effectively by the DL-EPR test using a solution 1 mol·L⁻¹ H₂SO₄+1.5 mol·L⁻¹ HCl. No IGC susceptibility was observed in both BM and WM.

It was also found that the pitting corrosion resistance, passivation and repassivation abilities in hot artificial seawater decrease in the order of BM, WM and HAZ. Among the three zones of the weld joint, HAZ has the lowest pitting corrosion resistance primarily due to the weak sensitization (i.e., Cr-depletion) adjacent to the Cr₂N precipitates. Compared with BM, WM has a slightly lower pitting corrosion resistance mainly as a result of its higher δ phase content, but the difference between the two zones is small.

ACKNOWLEDGEMENTS

This work was jointly supported by National Natural Science Foundation of China and Baowu Steel Group Co. Ltd. (Grant Nos. 51571139 and U1660205).

References

1. J. Gong, Y. M. Jiang, B. Deng, J. L. Xu, J. P. Hu and J. Li, *Electrochim. Acta*, 55 (2010) 5077.
2. G. Fargas, M. Anglada and A. Mateo, *J. Mater. Process. Technol.*, 209 (2009) 1770.
3. M. Pohl, O. Storz and T. Glogowski, *Mater. Charact.*, 58 (2007) 65.
4. J. Gao, Y. Jiang, B. Deng, W. Zhang, C. Zhong and J. Li, *Electrochim. Acta*, 54 (2009) 5830.
5. H. M. Ezuber, A. El-Houd and F. El-Shawesh, *Desalination*, 207 (2007) 268.
6. J. K. Sahu, U. Krupp, R. N. Ghosh and H. J. Christ, *Mater. Sci. Eng. A*, 508 (2009) 1.
7. D. H. Kang and H. W. Lee, *Corros. Sci.*, 74 (2013) 396.
8. Z.Q. Zhang, H. Y. Jing, L. Y. Xu, Y. D. Han, L. Zhao and J. L. Zhang, *Appl. Surf. Sci.*, 394 (2017)

297.

9. M. A. García-Rentería, V. H. López-Morelos, R. García-Hernández, L. Dzib-Pérez, E.M. García-Ochoa and J. González-Sánchez, *Appl. Surf. Sci.*, 321 (2014) 252.
10. J. Nowacki and A. Lukojc, *Mater. Charact.*, 56 (2006) 436.
11. R. Badji, M. Bouabdalah, B. Bacroix, C. Kahloun, B. Belkessa and H Maza, *Mater. Charact.*, 59 (2008) 447.
12. Y.T. Sun, X.Y. Wu, X. Wu, J. Li and Y.M. Jiang, *Int. J. Electrochem. Sci.*, 11 (2016) 9666.
13. Y. Yang, Z. Wang, H. Tan, J. Hong, Y. Jiang, L. Jiang and J. Li, *Corros. Sci.*, 65 (2012) 472.
14. Z. Zhang, Z. Wang, Y. Jiang, H. Tan, D. Han, Y. Guo and J. Li, *Corros. Sci.*, 62 (2012) 42.
15. H.J. Kim, S.H. Jeon, S.T. Kim, I.S. Lee, Y.S. Park and K.T. Kim, *Corros. Sci.*, 87 (2014) 60.
16. S.T. Kim, S.H. Jang, I.S. Lee and Y.S. Park, *Corros. Sci.*, 53 (2011) 1939.
17. B.H. Lee, H.W. Lee and Y.T. Shin, *Int. J. Electrochem. Sci.*, 10 (2015) 7535.
18. Y. H. Yang, B. Yan, J. Li and J. Wang, *Corros. Sci.*, 53 (2011) 3756.
19. Y. taek Shin, H. soo Shin and H. woo Lee, *Met. Mater. Int.*, 18 (2012) 1037.
20. T. Chehuan, V. Dreilich, K. S. de Assis, F.V. de Sousa and O. R. Mattos, *Corros. Sci.*, 86 (2014) 268.
21. J. Olsson and M. Snis, *Desalination*, 205 (2007) 104.
22. C. Liu, M. Gong and X.W. Zheng, *Int. J. Electrochem. Sci.*, 13 (2018) 7432.
23. S. S. Xin and M. C. Li, *Corros. Sci.*, 81 (2014) 96.
24. J. M. Vitek and S. A. David, *Metall. Mater. Trans. A*, 16 (1985) 1521.
25. A. J. Ramirez, J. C. Lippold and S. D. Brandi, *Metall. Mater. Trans. A*, 34 (2003) 1575.
26. A. J. Ramirez, S. D. Brandi and J. C. Lippold, *Sci. Technol. Weld. Join.*, 9 (2004) 301.
27. S. Geng, J. Sun, L. Guo and H. Wang, *J. Manuf. Process.*, 19 (2015) 32.
28. S. Zhang, Z. Jiang, H. Li, H. Feng and B. Zhang, *J. Alloys Compd.*, 695 (2017) 3083.
29. P. Erazmus-Vignal, V. Vignal, S. Saedlou and F. Krajcarz, *Corros. Sci.*, 99 (2015) 194.
30. J. O. Nilsson, L. Karlsson and J. O. Andersson, *Mater. Sci. Technol.*, 11 (2013) 276.
31. Z. Zhang, H. Zhao, H. Zhang, J. Hu and J. Jin, *Corros. Sci.*, 121(2017) 22.

© 2019 The Authors. Published by ESG (www.electrochemsci.org). This article is an open access article distributed under the terms and conditions of the Creative Commons Attribution license (<http://creativecommons.org/licenses/by/4.0/>).